A Management Circuit with Upconversion Oscillation Technology for Electric-Field Energy Harvesting

Jiajia Zhang, Ping Li, Yumei Wen, Feng Zhang, and Chao Yang

***Abstract*—Traditional *LC* resonance circuit can continuously and efficiently accumulate energy from the harvester at optimal impedance matching. Due to electric-field frequency (50 Hz, in China) and small equivalent capacitance (tens or hundreds of picofarads) of electric-field capacitive harvester, it is difficult to manufacture a huge transformer with a large inductance (>10 000 H) to optimally match the capacitive harvester. An upconversion oscillation circuit with a smaller size transformer around high-voltage power line is proposed to achieve efficient electric-field energy harvesting in this paper. The power-frequency output signal is transformed into higher frequency oscillation signal in the upconversion circuit consisting of the switch and the transformer. In this case, optimal impedance matching with the smaller size transformer is realized. Therefore, weak energy from harvester is fast accumulated into the storage capacitor by using the upconversion oscillation circuit. For a 10-kV power line, the upconversion maximum charging power reaches 663 μW in experiment. Due to optimal impedance matching in the upconversion oscillation circuit, the maximum harvesting efficiency is increased from 3% to 90.5%, compared with the traditional harvesting method. While the voltage across the storing capacitor is 3.26 V, the instantaneous discharge circuit can drive a wireless sensor node with an output power of 110 mW.**

***Index Terms*—Electric-field energy harvesting, high-frequency oscillation, power line, upconversion, wireless sensor node.**

I. Introduction

With the development of the low-power miniature CMOS, the wireless sensor networks have been used in wider fields, such as the monitoring of the harsh environment, the building structure, and the medical implants. A wireless sensor node powered by a battery with a limited energy hardly works for long time. In many applications, wireless sensor nodes are distributed in remote/dangerous regions or are embedded in detected objects such as buildings. In these cases, replacements of batteries for the wireless sensor nodes are difficult. A promising alternative solution to batteries is the use of energy harvesters that convert ambient energies within their environment into electrical energy. Many ambient energies such as solar energy [1], [2], vibrational energy [3]–[6], wind energy [7]–[10], and electromagnetic energy [11]–[12] are harvested for electronic systems. In remote areas or complex regions, it is attractive to scavenge ambient energies for autonomous wireless sensor networks to monitor some parameters such as temperature, inclination, aging, and icing of high-voltage power line. The induced electromagnetic field around the high-voltage power line can provide enough energy for a wireless sensor node with power consumption of hundreds of microwatts by using an instantaneous discharging circuit. According to Faraday's law of induction, the magnetic coil is used to harvest the magnetic-field energy induced by the current flowing through the wire [13], [14], but this energy source is unstable for the weak current. Due to the stable electric field around the power line, electric-field energy harvesting can be achieved on a high-voltage power line.

From the principle of a capacitance voltage divider, the cylindrical capacitive harvester is presented to harvest electric-field energy around a high-voltage power line [15], [16]. In order to obtain the required harvesting power, a voltage transformer connected directly to the harvester is proposed to achieve impedance transformation according to the output impedance of the harvester. Because the optimal impedance matching between the voltage transformer and the harvester is not realized, the efficiency of energy harvesting is only 3% [16]. In order to obtain the highest efficiency of energy harvesting, the primary inductance impedance of the transformer must be the conjugation of the equivalent impedance of harvester. For example, the traditional *LC* resonance matching circuit is proposed to obtain a maximum power from energy harvester [17], [18]. In consideration of the general length (tens of centimeters) and more output power of the harvester, the capacitance between the harvester on power line and the ground is several picofarads, and the equivalent capacitance of the harvester is tens or hundreds of picofarads. However, due to electric-field frequency (50 Hz, in China) and small equivalent capacitance of the capacitive harvester, the transformer requires a huge inductance (>10 000 H) to optimally match the equivalent impedance of the harvester in the traditional *LC* resonance circuit. Not only it is difficult to realize in small size, but also the harvesting efficiency is diminished due to the distributed capacitance of the transformer with the huge inductance. In order to avoid the manufacture difficulty of the transformer with the huge inductance in the traditional *LC* resonance circuit, an upconversion resonance circuit, including two high-frequency *LC* resonance loops and a switch, is designed [19]. When the control frequency of the switch is equal to the *LC* resonance frequency, the optimal impedance matching

Manuscript received March 19, 2015; revised June 5, 2015 and August 31, 2015; accepted October 2, 2015. Date of publication October 26, 2015; date of current version March 2, 2016. This work was supported by the National Natural Science Foundation of China under Grants 61531008 and 61374217. Recommended for publication by Associate Editor J. A. Cobos.

The authors are with the Research Center of Sensors and Instruments, College of Optoelectronic Engineering, Chongqing University, Chongqing 400044, China (email: liping@cqu.edu.cn).

Color versions of one or more of the figures in this paper are available online at http://ieeexplore.ieee.org.

Digital Object Identifier 10.1109/TPEL.2015.2491960

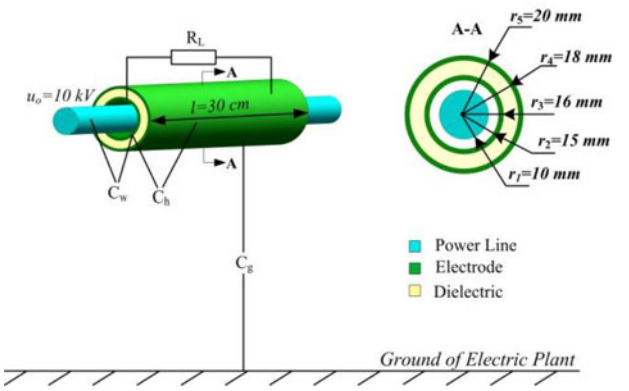

Fig. 1. Structure of electric-field energy harvesting.

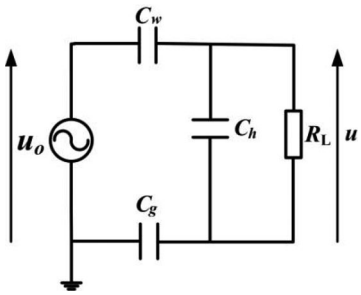

Fig. 2. Equivalent circuit of energy harvesting.

is realized. However, because of small equivalent capacitance of the capacitive harvester, the stray capacitance of switch cannot be neglected, and impulse response is not obtained in the output loop of the upconversion resonance circuit at the turn-off moment. Therefore, the high-efficiency energy harvesting cannot be achieved by using the upconversion resonance circuit.

In this paper, aiming at improving the efficiency of electric-field energy harvesting, an upconversion oscillation circuit, including a small-size ($50 \times 20 \times 20$ mm^3) transformer and a bidirectional switch consisting of two MOSFETs, is proposed. Through turning on/off the switch periodically, the power-frequency voltage signal across the harvester is converted into the higher frequency output signal, including two alternate oscillations. Because of the alternate oscillations, optimal impedance matching can be realized by using the upconversion oscillation circuit. The upconversion oscillation circuit with a small-size transformer can efficiently accumulate the electric-field energy from the harvester.

II. Electric-Field Energy Harvester

The noncontacting cylindrical harvester for supplying wireless monitoring device is shown in Fig. 1. The cylindrical harvester is used as a capacitive voltage divider to harvest electric field energy. The harvester comprises a tubular inner electrode, a tubular outer electrode, and a dielectric material between the inner electrode and the outer electrode. R_L is the load resistance. Fig. 2 shows the equivalent circuit of energy harvesting. Three capacitors C_w (power line to inner electrode), C_h (inner electrode to outer electrode), and C_g (outer electrode to ground of the electric plant) are connected in series. C_w, C_h, and C_g are described by [16]

$$\begin{cases} C_w = \dfrac{2\pi\varepsilon_0 l}{\ln(r_2/r_1)} \\ C_h = \dfrac{2\pi\varepsilon_0\varepsilon_r l}{\ln(r_4/r_3)} \\ C_g = \dfrac{2\pi\varepsilon_0 l}{\ln(2h/r_5)} \end{cases} \tag{1}$$

where ε_0, ε_r, r_1, and h represent the permittivity of vacuum, the relative dielectric constant of the dielectric, the radius of the power line, and the height from outer electrode to ground, respectively.

From Fig. 2, the voltage u across the load is given by

$$u = \frac{R_L/(1+j\omega_p C_h R_L)}{R_L/(1+j\omega_p C_h R_L) + 1j\omega_p C_w + 1/j\omega_p C_g} u_o \tag{2}$$

where u_o and ω_p represent the power-line phase-ground rms voltage and the angular frequency of the power-line voltage, respectively. For load resistance the obtainable power can be expressed as

$$P = \frac{|u|^2}{R_L}. \tag{3}$$

When $\partial P/\partial R_L = 0$, the optimal load resistance $R_{L(\mathrm{opt})}$ can be calculated by (4). Thus, the maximal power ($P_{\max}$) can be obtained at $R_L = R_{L(\mathrm{opt})}$ (5) at bottom of the page

$$R_{L(\mathrm{opt})} = \frac{\ln(r_4/r_3)\ln(2r_2h/r_1r_5)}{2\pi\varepsilon_0 l\omega_p[\ln(r_4/r_3) + \varepsilon_r \ln(2r_2h/r_1r_5)]} \tag{4}$$

From (5), the maximum output power ($P_{\max}$) of the harvester increases with the rms voltage (u_o) of the power line, the length (l) of the harvester, r_4 and r_5 (see Fig. 1); and decreases with increasing r_2, r_3 and ε_r. Meanwhile, in order to obtain more power from the harvester, the size of the harvester must be increased as much as possible.

In experiment, as shown in Fig. 1, the length (l) of the harvester and r_1, r_2, r_3, r_4, and r_5 are 30 cm and 10, 15, 16, 18, and 20 mm, respectively. The inner and outer electrodes are separated by the insulation paper with a relative dielectric constant (ε_r) of 1.56, and thus, the capacitance (C_h) of the harvester is 211.7 pF. The phase-to-ground rms voltage of the power line is 10 kV. General height of 10 kV power line is above 8 m. From (5), the maximum output power is $P_{\max} \propto 1/[0.19(\ln h)^2 + 3.4\ln h + 12.7]$. For example, the maximum output powers ($P_{\max}$) at the power-line heights of 8 and 16 m are 0.62 times and 0.54 times of that at the power-line height of 1 m, respectively. $P_{\max}$ decreases slowly with the fast

$$P_{\max} = \frac{2\pi\varepsilon_0 l\omega_p u_o^2 \cdot [\ln(r_4/r_3)]^2}{[\ln(r_4/r_3) + \varepsilon_r \ln(2r_2h/r_1r_5)] \cdot [\ln(r_4/r_3)\ln(2r_2h/r_1r_5) + 1]} \tag{5}$$

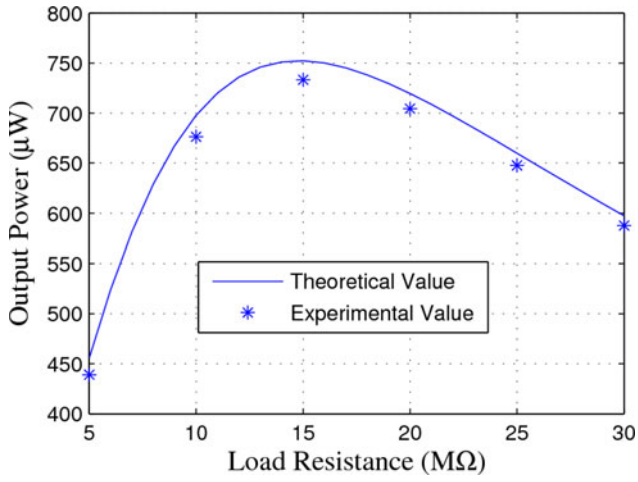

Fig. 3. Output power versus load resistance for values of experimental parameters ($u_o = 10$ kV, $h = 1$ m, $l = 30$ cm, $r_1 = 10$ mm, $r_2 = 15$ mm, $r_3 = 16$ mm, $r_4 = 18$ mm, $r_5 = 20$ mm, and $\varepsilon_r = 1.56$).

increase of the height (h) of the power line. The height of a 10-kV power line varies with the different environment. The results of the electric-field energy harvesting at $h > 8$ m can be calculated according to the experimental results at $h = 1$ m. For the convenient test in experiment, the height of the 10-kV power line is set to 1 m. As shown in Fig. 3, the theoretical value agrees well with the experimental results. From Fig. 3, the theoretical and experimental output powers increase first and then decrease with the increase of the load resistance. Their maximum output powers are 750 and 733 μW at the load resistance of about 15 MΩ, respectively. In order to obtain the maximum charging power (which equals 733 μW), the traditional *LC* resonance circuit is proposed, as shown in Fig. 4. L_{r1} and L_{r2} are the primary inductance and the secondary inductance of the transformer, respectively. In the traditional *LC* resonance circuit ($C_{st} = 0.47$ F), because $1/\sqrt{L_{r1}C_h} = 1/\sqrt{L_{r2}C_{r2}} = \omega_p$, the transformer (turn ratio $n = 50$) with $L_{r1} = 47910$ H and $L_{r2} = 19$ H is required according to the experimental values ($h = 1$ m and $u_o = 10$ kV) and the calculated values ($C_g = 3.6$ pF, $C_h = 211.7$ pF, and $C_w = 41.1$ pF) of parameters. The traditional circuit requires a huge transformer with a large primary inductance (47 910 H). Obviously, it is very difficult to realize in small size.

III. Management Circuit

The management circuit for the electric-field energy harvesting is composed of an upconversion oscillation circuit, a control circuit, a rectifier, a storing capacitor C_{st}, an instantaneous discharging circuit, and a wireless sensor node, as shown in Fig. 5. In the upconversion oscillation circuit, the bidirectional switch *S* consists of two MOSFETs NDF03N60Z (ON Semiconductor Inc.) with a small conduction resistance (3.6 Ω), a large current (2.6 A) and a high breakdown voltage (600 V). The upconversion oscillation circuit with a small-size transformer can convert power-frequency voltage signal across the harvester into higher frequency signal. The rectifier transfers the higher frequency ac signal into the dc signal for the main storing capacitor C_{st}, and then energy from the harvester with the weak output power

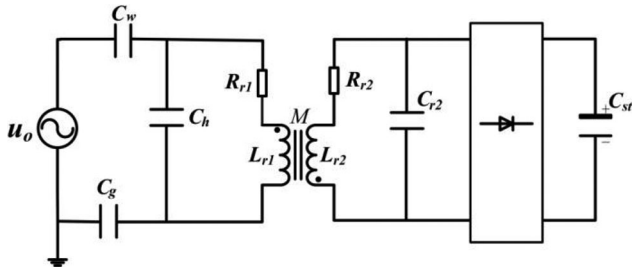

Fig. 4. Traditional *LC* resonance circuit for electric-field energy harvesting.

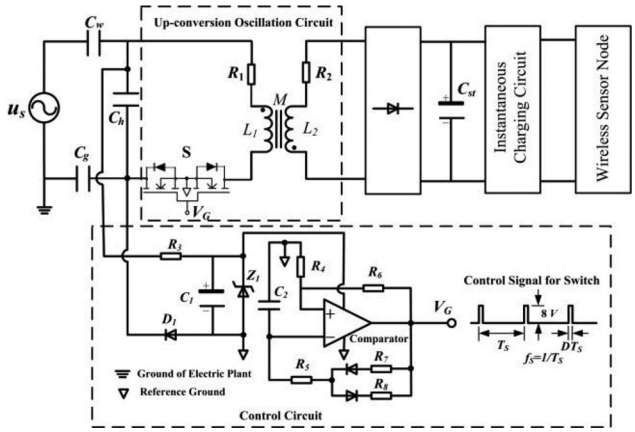

Fig. 5. Management circuit of electric-field energy harvesting.

(733 μW) can be continuously and efficiently accumulated to C_{st} in a long period. The instantaneous discharging circuit with a LDO S1313 (Seiko Inc.) is used to provide a higher output power and a stable voltage for the wireless sensor node with a high consumption power (hundreds of microwatts) in a very short time. The micropower control circuit with a low power consumption of about 6 μW, consisting of a comparator MAX924 (Maxim Integrated Inc.), a half-wave rectifier bridge (D_1), a voltage-regulator diodes (Z_1), resistors, and capacitors, can produce the pulse signal for the upconversion oscillation circuit. In the control circuit, the half-wave rectifier bridge (D_1) transfers the ac signal into the dc signal for the capacitor $C_1(100\ \mu F)$. By using the voltage-regulator diode Z_1, a stable voltage is obtained for the comparator. A pulse signal with the voltage amplitude (8 V) is produced for the switch.

A. Upconversion Oscillation Circuit

In order to avoid the large-size transformer and realize optimal impedance matching, the upconversion oscillation circuit composed of the harvester, the smaller size transformer, and the bilateral switch *S* (consisting of two MOSFETs) is designed for harvesting electric-field energy, as shown in Fig. 5. L_1 and L_2 are the primary and secondary inductances of the transformer, respectively. *M* is the mutual inductance of the transformer. R_1 and R_2 are the resistances of the primary and the secondary coils in the transformer, respectively. u_s is the phase-to-ground voltage of the power line.

High voltage on the power line can be expressed as

$$u_s(t) = \sqrt{2}u_o \sin(\omega_p t) \tag{6}$$

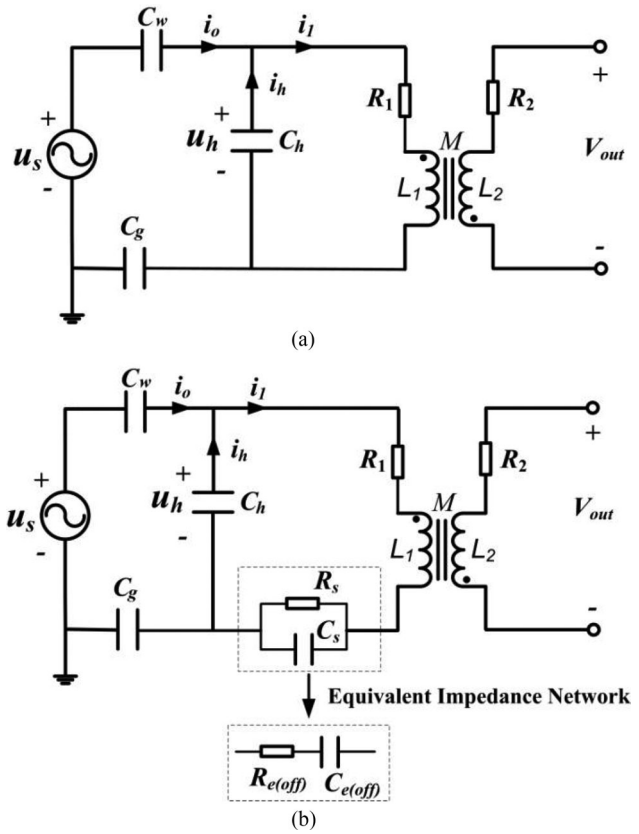

Fig. 6. Equivalent upconversion oscillation circuits. (a) Switch-on time and (b) Switch-off time.

where u_o is the phase-to-ground rms voltage of the power line. The switch *S* driven by the control circuit is turned on/off periodically. T_s and *D* are the switch period and the switch duty cycle, respectively. The switch frequency is $f_s = 1/T_s$. $t_1 \le t \le t_2$ and $t_2 \le t \le t_1 + T_s$ are the time windows when the switch *S* is turned on and off, respectively. The turn-on moment is defined as $t_1 = t_0 + nT_s$, the turn-off moment is defined as $t_2 = t_1 + DT_s$, n is a nonnegative integer, and t_0 is the first turn-on moment of the switch.

The equivalent upconversion oscillation circuits in the turn-on/off time are shown in Fig. 6. From Fig. 6, the switch *S* is replaced by the wire in the turn-on time. In the turn-off time, the switch *S* can be substituted by the series network of the switch-off capacitance (C_s) and the switch-off resistance (R_s). Based on equivalent impedance, the series network of the switch-off capacitance (C_s) and the switch-off resistance (R_s) is equivalent to the parallel connection of the equivalent switch-off capacitance $(C_{e(\mathrm{off})})$ and the equivalent switch-off resistance $(R_{e(\mathrm{off})})$. $C_{e(\mathrm{off})} = C_s + 1/\omega^2 C_s R_s^2$ and $R_{e(\mathrm{off})} = R_S/1 + \omega^2 C_s^2 R_s^2$, where ω is the angular frequency of the voltage across the switch. In turn-off time, the harvester is charged by the high voltage source. Because $C_{e(\mathrm{off})}$ (tens of picofarads) is much smaller than C_h (hundreds of picofarads) in Fig. 6 (b), $i_h(t) \approx i_o(t)$. The voltage across the harvester at the turn-on moment t_1 can be expressed by

$$u_h(t_1) = \begin{cases} u_h(t_0), & n = 0 \\ u_h(t_1 - T_{\mathrm{off}}) + \int_{t_1 - T_{\mathrm{off}}}^{t_1} i_h(t)d, & n \ge 1 \end{cases} \tag{7}$$

where $u_h(t_0)$ and $u_h(t_1 - T_{\mathrm{off}})$ are the voltages across the harvester at the moments $t = t_0$ and $t = t_1 - T_{\mathrm{off}}$, respectively. $T_{\mathrm{off}} = (1 - D)T_s$. $i_h(t) = \sqrt{2}\omega_p C_w C_g u_o \sin(\omega_p t)/(C_w C_h + C_h C_g + C_g C_w)$ is the charging current through the harvester in the turn-off time.

From Fig. 6, the current i_1 through the primary inductance L_1 is the sum of the current i_h and the current i_o. In the turn-on time, because $R_1/(2L_1) < 1/\sqrt{L_1 C_h}$, a damped oscillation current (i_h) is produced in the $R_1 - C_h - L_1$ circuit. i_o is a power-frequency current produced by the high-voltage source. At the power frequency, the impedance of the primary inductance L_1 in the small-size transformer is far less than the impedance of C_h, the impedance of C_w, and the impedance of C_g. The differential equation of the voltage across C_h is expressed as

$$L_1 C_h \frac{d^2 u_h}{dt^2} + R_1 C_h \frac{du_h}{dt} + u_h = 0. \tag{8}$$

According to (8), the current $i_h = C_h\, du_h/dt$ and the initial voltage $u_h(t_1)$ across the harvester, i_1 in the turn-on time window $(t_1 \le t \le t_2)$ can be approximately expressed by

$$\begin{cases} i_1(t) = i_h(t) + i_o(t) = \dfrac{u_h(t_1)}{\omega_1 L_1} e^{-\alpha_1 (t - t_1)} \sin[\omega_1 (t - t_1)] + i_o(t) \\ i_o(t) = \dfrac{\sqrt{2}(C_w + C_g) u_o}{\omega_p C_w C_g} \cos(\omega_p t) \end{cases} \tag{9}$$

where $\omega_{r1} = \sqrt{1/(L_1 C_h)}$ is the resonance angular frequency in the turn-on time. $\alpha_1 = R_1/2L_1$ is the attenuation coefficient in the turn-on time. $\omega_1 = \sqrt{\omega_{r1}^2 - \alpha_1^2}$ is the oscillating angular frequency in the turn-on time.

In the turn-off time, another damped oscillation occurs in the primary loop. The impedance of $R_s - C_s$ parallel network is equal to the impedance of $C_{e(\mathrm{off})} - R_{e(\mathrm{off})}$ series network, and hence, the $R_s - C_s$ parallel network can be replaced by the $C_{e(\mathrm{off})} - R_{e(\mathrm{off})}$ series network. Being similar to the analysis in the turn-on time, the differential equation of the sum (u_e) of the voltage (u_h) across C_e and the voltage $(u_{C_{e(\mathrm{off})}})$ across $C_{e(\mathrm{off})}$ is expressed as

$$L_1 C_e \frac{d^2 u_e}{dt^2} + R_e C_e \frac{du_e}{dt} + u_e = 0 \tag{10}$$

where $C_e = C_{e(\mathrm{off})} C_h/(C_{e(\mathrm{off})} + C_h)$, $R_e = R_1 + \mathrm{R}_{e(\mathrm{off})}$, and $u_e = u_h + u_{C_{e(\mathrm{off})}}$. According to (10), the current $i_h = C_e du_e/dt$ and the initial voltage $u_e(t_2) = u_h(t_1)\sin(\omega_1 DT_s) e^{-\alpha_1 DT_s}$ across the harvester and i_1 in the turn-off time window $(t_2 \le t \le t_1 + T_s)$ can be approximately expressed by

$$\begin{cases} i_1(t) = i_h(t) + i_o(t) = I_m\, e^{-\alpha_2 (t - t_2)} \cos[\omega_2 (t - t_2] + i_o(t) \\ i_o(t) = \dfrac{\sqrt{2}\omega_p C_w C_g (C_h + C_{e(\mathrm{off})}) u_o}{C_w (C_h + C_{e(\mathrm{off})}) + (C_h + C_{e(\mathrm{off})}) C_g + C_g C_w} \cos(\omega_p t) \\ I_m = \dfrac{u_e(t_2)}{\omega_1 L_1} \end{cases} \tag{11}$$

where $\omega_{r2} = \sqrt{1/L_1 C_e}$is the resonance angular frequency in the turn-off time. $\alpha_2 = R_{\mathrm{e}}/2L_1$ is the attenuation coefficient in the turn-off time. $\omega_2 = \sqrt{\omega_{r2}^2 - \alpha_2^2}$ is the oscillating angular frequency in the turn-off time. From (9) and (11), a new higher

TABLE I
PARAMETERS OF COMPONENTS IN UPCONVERTION OSCILLATION CIRCUIT

Symbol	Quantity	Value
L_1	Primary inductance of transformer	3.63 H
L_2	Secondary inductance of transformer	36.3 mH
R_1	Resistance of primary coil	122 Ω
R_2	Resistance of secondary coil	15 Ω
M	Mutual inductance of transformer	0.36 H
$C_{e(\text{off})}$	Equivalent off capacitance of switch	40 pF
$R_{e(\text{off})}$	Equivalent off resistance of switch	11 kΩ

frequency current signal with two oscillation frequencies is induced in the primary loop.

According to (9) and (11), the output voltage across the output inductor L_2 is given by (12), shown at bottom of the page, where $\varphi_1 = \arctan(\alpha_1/\omega_1)$and $\varphi_2 = \arctan(\alpha_2/\omega_2)$.

From (12), in the turn-on/off time, the output voltage is sum of alternating higher frequency oscillation voltage and alternating power-frequency voltage. The higher frequency peak voltage in turn-on/off time is directly proportional to the primary inductance (L_1), and inversely proportional to the mutual inductance (*M*). Therefore, by using a transformer with a smaller primary inductance and larger mutual inductance, higher oscillation voltages can be obtained.

According to (1) and the values ($h = 1$ m, $l = 30$ cm, $r_1 = 10$ mm, $r_2 = 15$ mm, $r_3 = 16$ mm, $r_4 = 18$ mm, $r_5 = 20$ mm, and $\varepsilon_r = 1.56$) of the parameters in Section II, the capacitances ($C_g = 3.6$ pF, $C_h = 211.7$ pF, and $C_w = 41.1$ pF) are obtained. According to the calculated capacitances and the parameters (as shown in Table I) of components in upconversion oscillation circuit, the theoretical power-frequency peak voltage (0.016 V) is far less than the theoretical higher frequency peak voltage (21 V) at the switch frequency of 200 Hz and the switch duty cycle of 5%. In this case, the higher frequency oscillation voltage signal possesses most of the energy, and the power-frequency voltage signal can be ignored. Theoretical output voltage (V_{out}) across L_1 and current (i_1) through primary loop are shown in Fig. 7. From Fig. 7, the power-frequency output voltage/current signals of the harvester are converted into the higher frequency output voltage/current signals with two oscillation frequencies by using the upconversion oscillation circuit, respectively.

Fig. 8 shows the output voltage across the output inductor in the upconversion oscillation circuit at the switch frequency of 200 Hz and the switch duty cycle of 5% in experiment. From Fig. 8, the power-frequency output signal of the harvester is transformed into the envelope signal with the envelope frequency of 200 Hz. Each envelope includes two alternating high-

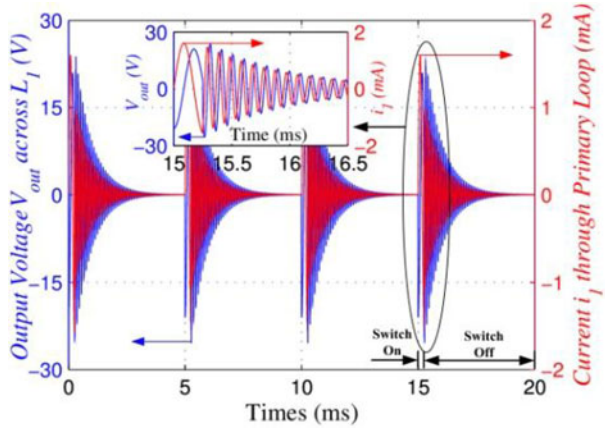

Fig. 7. Theoretical output voltage (V_{out}) across L_1 and current (i_1) through primary loop for values of frequency upconversion oscillation circuit parameters ($u_s = 14.14\sin(314t)$ kV, $C_g = 3.6$ pF, $C_h = 211.7$ pF, $C_w = 41.1$ pF, $L_1 = 3.63$ H, $L_2 = 36.3$ mH, $R_1 = 122\ \Omega$, $R_2 = 15\ \Omega$, $M = 0.36$ H, $C_{e(\text{off})} = 40$ pF, $R_{e(\text{off})} = 11$ kΩ, $f_s = 200$ Hz, and $D = 5\%$).

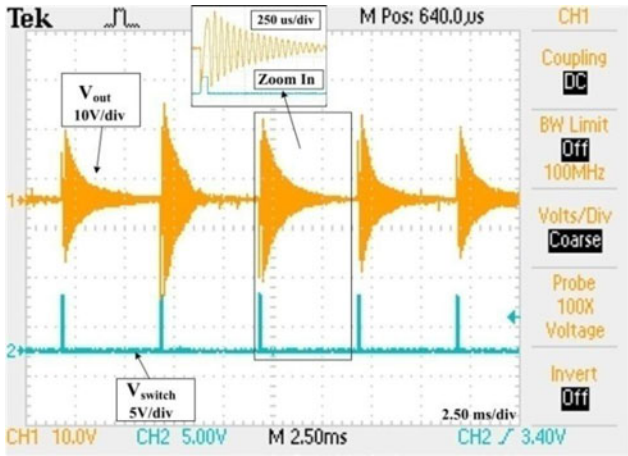

Fig. 8. Output waveform of the upconversion oscillation circuit for values of circuit parameters ($u_s = 14.14\sin(314t)$ kV, $h = 1$ m, $l = 30$ cm, $r_1 = 10$ mm, $r_2 = 15$ mm, $r_3 = 16$ mm, $r_4 = 18$ mm, $r_5 = 20$ mm, $\varepsilon_r = 1.56$, $L_1 = 3.63$ H, $L_2 = 36.3$ mH, $R_1 = 122\ \Omega$, $R_2 = 15\ \Omega$, $M = 0.36$ H, $C_{e(\text{off})} = 40$ pF, $R_{e(\text{off})} = 11k\Omega$, $f_s = 200$ Hz, and $D = 5\%$).

frequency oscillation voltage signals. The higher frequency oscillation voltage amplitude decreases with duration time at turn-off time. Experimental results verify the theoretical analysis. The voltage amplitude of the turn-off time is higher than that of the turn-on time, and thus, a stronger charging energy can be obtained.

$$V_{\text{out}} = -M\frac{di_1}{dt} = \begin{cases} -\dfrac{\omega_{r1}M}{\omega_1 L_1}u_h(t_1)e^{-\alpha_1(t-t_1)}\cos[\omega_1(t-t_1)+\varphi_1] - \dfrac{\sqrt{2}\omega_p^2 C_w C_g M u_o}{C_w + C_g}\sin(\omega_p t)(t_1 \le t \le t_2) \\ \omega_{r2}MI_m e^{-\alpha_2(t-t_2)}\sin[\omega_2(t-t_2)+\varphi_2] - \dfrac{\sqrt{2}\omega_p^2 C_w C_g (C_h + C_{e(\text{off})})M u_o}{C_w(C_h + C_{e(\text{off})}) + (C_h + C_{e(\text{off})})C_g + C_g C_w}\sin(\omega_p t)(t_2 \le t \le t_1 + T_s) \end{cases} \tag{12}$$

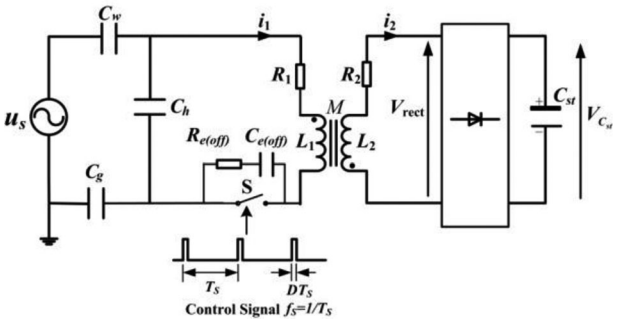

Fig. 9. Equivalent circuit of charging for a storing capacitor by the upconversion oscillation circuit.

B. Charging for a Storing Capacitor

As shown in Fig. 9, the ac output signal from the upconversion matching circuit is transferred into the dc signal by the rectifier bridge, and the charging for the storing capacitor ($C_{\rm st}$) is realized. The rectifier bridge is closed, and the charging current through the storing capacitor can be produced while the voltage ($V_{\rm rect}$) across the secondary coil is higher than the voltage ($V_{C_{\rm st}}$) across the storing capacitor; whereas the rectifier bridge is open, and the charging current through the storing capacitor is cutoff. The voltage across the rectifier bridge is ignored, because the voltage ($\sim$0.1 V) across the rectifier bridge is much less than that across the storing capacitor (>1 V).

From Fig. 8, at the switch frequency of 200 Hz and the switch duty cycle of 5%, the main charging energy is possessed by the converted high-frequency signal during the switch-off time. We ignore the output signal during the switch-on time. Fig. 10 shows the voltage ($V_{\rm rect}$) across the rectifier bridge, the current (i_2) through the rectifier bridge, and the charging current ($i_{C_{\rm st}}$). According to [20], the charging current of the storing capacitor can be described by

$$i_{C_{\rm st}} = \frac{Mi_1(t)}{L_2}, \qquad \Omega \le \omega t \le \pi - \Omega \tag{13}$$

where Ω is the conduction angle of the rectifier bridge. The average charging current of the storing capacitor $C_{\rm st}$ can be described by

$$\bar{i}_{C_{\rm st}} = \frac{1}{\pi}\int_{\Omega}^{\pi-\Omega} i_{C_{\rm st}}\,d\theta = -\frac{2\omega_2 MI_m}{\pi\omega_{r2}L_2}\sin(\Omega+\varphi_2)e^{(-\alpha_2\Omega/\omega_2)} + \frac{2\omega_2^2 MI_m}{\pi^2\omega_{r2}^2 L_2}e^{(-\pi\alpha_2/2\omega_2)}. \tag{14}$$

When the rectifier is open, the voltage across L_2 is equal to the voltage across the storing capacitor $C_{\rm st}$

$$V_{C_{\rm st}} = V_{L_2} = \omega_{r2}MI_m e^{(-\alpha_2\Omega/\omega_2)}\sin(\Omega+\varphi_2). \tag{15}$$

The voltage across the storing capacitor can be expressed by

$$C_{\rm st}\frac{dV_{C_{\rm st}}}{dt} = \bar{i}_{C_{\rm st}}. \tag{16}$$

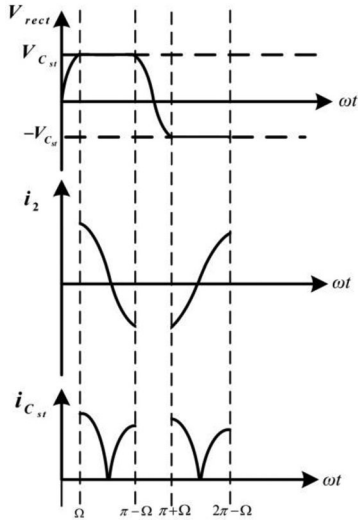

Fig. 10. Voltage across rectifier bridge, current through rectifier bridge, and charging current.

From (14), (15), and (16), the charging process of storing capacitor can be expressed by

$$V_{C_{\rm st}}(t) = \frac{\omega_2^2 MI_m}{\pi\omega_{r2}}e^{-\frac{\pi\alpha_2}{2\omega_2}}\left(1-e^{-\frac{2t}{\pi\omega_{r2}L_2C_{\rm st}}}\right). \tag{17}$$

From (17), the charging voltage across the storing capacitor increases with an exponential function. The charging time constant is directly proportional to the capacitance of the storing capacitor, the secondary inductance, and the resonant frequency of the primary loop in the turn-off duration.

According to (17), the charging voltage increases faster with a smaller capacitance of storing capacitor. However, more energy in the larger storing capacitor can be obtained at its output voltage (that is, the relatively stable input voltage of $3.2-3.5$ V across the load with the power consumption of several hundred milliwatts, including the instantaneous-discharge circuit and the wireless sensor node). Hence, an appropriate storing capacitor of 0.47 F ($17.3\times 9\times 14.5$ mm^3) with the acceptable voltage variation of $0-5$ V for a wireless sensor node with power consumption of hundreds of microwatts is used.

At different switch frequency and duty cycle, the experimental charging voltage of the storing capacitor in 1 min is shown in Fig. 11. From Fig. 11, the experimental charging voltage of the storing capacitor increases first and then decreases with the increase in the switch frequency, and the same variation tendency of the experimental charging voltage versus the switch duty cycle is obtained. The fastest charging process of the storing capacitor ($C_{\rm st}=0.47$ F) can be achieved at the optimal switch frequency of 200 Hz and switch duty cycle of 5%.

At the optimal switch frequency of 200 Hz and switch duty cycle of 5%, the charging process of the storing capacitor by using the upconversion oscillation circuit is achieved in experiment, as shown in Fig. 12. It is similar to the charging process of the first-order *RC* circuit. The experimental results present the similar trend of the theoretical charging process of the storing capacitor. Fast charging process of the storing capacitor is obtained by using upconversion oscillation circuit. By using the

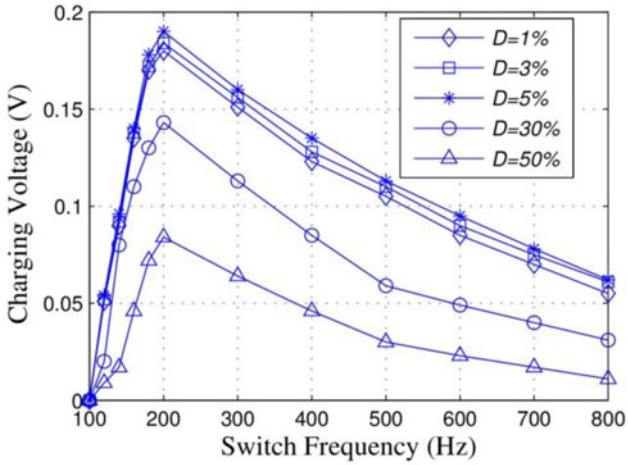

Fig. 11. Experimental charging voltage of the storing capacitor at different switch frequencies and duty cycles in 1 min for values of circuit parameters ($u_s = 14.14\sin(314t)$ kV, $h = 1$ m, $l = 30$ cm, $r_1 = 10$ mm, $r_2 = 15$ mm, $r_3 = 16$ mm, $r_4 = 18$ mm, $r_5 = 20$ mm, $\varepsilon_r = 1.56$, $L_1 = 3.63$ H, $L_2 = 36.3$ mH, $R_1 = 122\ \Omega$, $R_2 = 15\ \Omega$, $M = 0.36$ H, $C_{\rm st} = 0.47$ F, $C_{e(\rm off)} = 40$ pF, and $R_{e(\rm off)} = 11$ kΩ).

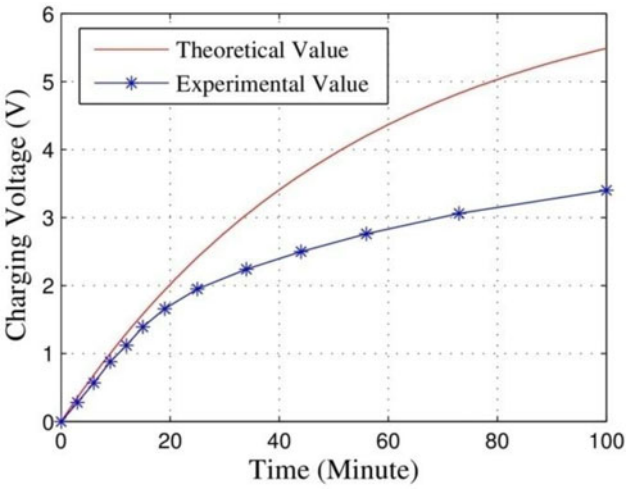

Fig. 12. Charging process of a storing capacitor for values of circuit parameters ($u_s = 14.14\sin(314t)$ kV, $h = 1$ m, $l = 30$ cm, $r_1 = 10$ mm, $r_2 = 15$ mm, $r_3 = 16$ mm, $r_4 = 18$ mm, $r_5 = 20$ mm, $\varepsilon_r = 1.56$, $L_1 = 3.63$ H, $L_2 = 36.3$ mH, $R_1 = 122\ \Omega$, $R_2 = 15\ \Omega$, $M = 0.36$ H, $C_{\rm st} = 0.47$ F, $C_{e(\rm off)} = 40$ pF, $R_{e(\rm off)} = 11$ kΩ, $f_s = 200$ Hz, and $D = 5\%$).

instantaneous discharge circuit with the low-dropout (LDO), a stable voltage can be provided to the wireless sensor node. The wireless sensor node is composed of a humidity and temperature sensor (type SHT11) with a typical voltage of 3.3 V and current of 0.9 μA, a high-speed low-power 8-bit processing (microprocessor, type ATmega32L) with a typical voltage of 3 V and current of 1.1 mA, and a low-power transceiver (type CC1100) with a typical voltage of 3 V and current of 1.9 μA. Because the leakage current ($I_{\rm leak} = KC_{\rm st}V_{C_{\rm st}}$) is proportion to the charging voltage across the storing capacitor, the theoretical charging speed is faster than the experimental charging speed, and the deviation between the theoretical results and the experimental results varies with the charging time. Because the measured leakage current ($I_{\rm leak} = 15\ \mu$A) through the storing capacitor

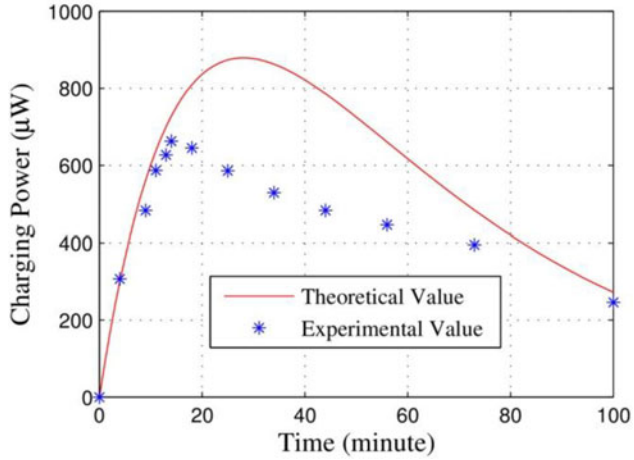

Fig. 13. Charging power of a storing capacitor as a function of charging time for values of circuit parameters ($u_s = 14.14\sin(314t)$ kV, $h = 1$ m, $l = 30$ cm, $r_1 = 10$ mm, $r_2 = 15$ mm, $r_3 = 16$ mm, $r_4 = 18$ mm, $r_5 = 20$ mm, $\varepsilon_r = 1.56$, $L_1 = 3.63$ H, $L_2 = 36.3$ mH, $R_1 = 122\ \Omega$, $R_2 = 15\ \Omega$, $M = 0.36$ H, $C_{e(\rm off)} = 40$ pF, $R_{e(\rm off)} = 11$ kΩ, $C_{\rm st} = 0.47$ F, $f_s = 200$ Hz, and $D = 5\%$).

(Type PB-5R0V474-R) at the charging voltage of 3.4 V is ignored, the deviation ($\Delta_1 = \omega_2 L_2 I_{\rm leak}$) of 0.5 V is caused. According to the parameters of the MOS (Type NDF03N60Z), the deviation $\Delta_2 = P_{\rm Sloss}/I_{\rm leak} = (U_{\rm on}Q_g f_s/I_{\rm leak}) = (6\,\text{V} \times 12\,\text{nC} \times 200\,\text{Hz}/15\,\mu\text{A}) = 0.9\,\text{V}$, where $P_{\rm Sloss}$, $U_{\rm on}$, Q_g, and f_s are the loss power, the turn-on voltage, the gate charge, and the switch frequency of the MOS, respectively. Besides, the threshold voltage (0.1 V) of the rectifier bridge consisting of four diodes (Type 1N60P) is ignored. Thus, there is a total deviation of 1.5 V between experimental and theoretical results at the charging voltage of 3.4 V.

The charging power of the storing capacitor can be calculated by

$$P_{C_{\rm st}}(t) = \frac{dW_{C_{\rm st}}(t)}{dt} \tag{18}$$

$$W_{C_{\rm st}}(t) = \frac{1}{2}C_{\rm st}[V_{C_{\rm st}}(t)]^2. \tag{19}$$

The variation of the charging power of the storing capacitor versus the charging time is shown in Fig. 13. The charging power increases first and then decreases with increase of the charging time. The experimental maximum charging power of 663 μW can be obtained at the charging voltage of 1.4 V.

By using the upconversion oscillation circuit (see Fig. 9), the variation of the experimental charging power of the storing capacitor versus the charging voltage is shown in Fig. 14. From Fig. 14, the charging power increases first and then decreases with increase of the storing voltage. The maximum experimental charging power reaches 663 μW at the charging voltage of 1.4 V. The harvesting efficiency ($\eta = P_{C_{\rm st}}/P_{\rm max}$) is defined as a ratio of the charging power ($P_{C_{\rm st}}$) of the storing capacitor ($C_{\rm st}$) to the maximum output power ($P_{\rm max}$, Fig. 3) of the harvester. Because the maximum charging power of the storing capacitor ($C_{\rm st}$) and the experimental maximum output power of the harvester at a load resistance of 15 MΩ without the proposed conversion

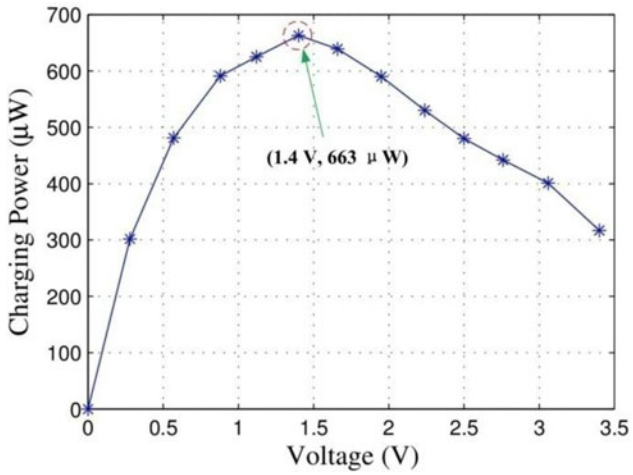

Fig. 14. Experimental charging power of storing capacitor as a function of charging voltage.

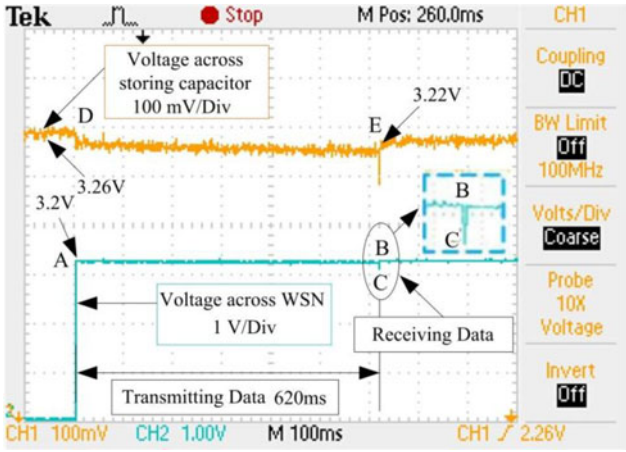

Fig. 15. Voltage waveforms across storing capacitor and wireless sensor node for electric-field energy harvesting.

system are 663 μW (see Fig. 14) and 733 μW (see Fig. 3), respectively, the maximum charging efficiency of 90.5% can be calculated by (20). In the previous work [16], according to the charging power (16.4 mW) of the storing capacitor and the maximum output power (540 mW) of the harvester at the load resistance of 300 MΩ, the harvesting efficiency is 3%. By using the upconversion oscillation circuit, the maximum harvesting efficiency is increased from 3% to 90.5%, compared with the previous method [16]

$$\eta_{\max} = \frac{P_{C_{\mathrm{st}}\max}}{P_{\max}} = \frac{663\,\mu\mathrm{W}}{733\,\mu\mathrm{W}} = 90.5\%. \tag{20}$$

IV. Experiment

A phase-to-ground root-mean-square voltage of 10 kV with a frequency of 50 Hz at a power line is produced by a high-voltage transformer. The designed tubular capacitive harvester is installed on the power line. The management circuitry with the upconversion oscillation technology and a storing capacitor of 0.47 F is connected to the harvester. An oscilloscope is used to measure the voltages across the storing capacitor and the wireless sensor node. First, the voltages across the storing capacitor and the wireless sensor node are obtained. Then the data of the wireless sensor node is achieved and displayed in computer at different transmission distances. The wireless sensor node is composed of a humidity and temperature sensor (type SHT11), a high-speed, low-power 8-bit processing (microprocessor, type ATmega32L) and a low-power transceiver (type CC1100). An LDO regulator (type S1313) is used to provide a stable voltage for the wireless sensor node. The wireless sensor node can work at different states: sleeping, receiving, and transmitting. The power of the receiving data is 20 mW at a receiving time of 620 ms, and the power of the transmitting data is 110 mW at a transmitting time of 5 ms. The necessary minimum energy of the wireless sensor node in a working cycle is

$$\begin{aligned} W = PT &= 20\,\mathrm{mW} \times 0.62\,\mathrm{s} + 110\,\mathrm{mW} \times 0.005\,\mathrm{s} \\ &= 12.85\,\mathrm{mJ}. \end{aligned} \tag{21}$$

Fig. 15 shows the voltage waveforms across the storing capacitor and the wireless sensor node with electric-field energy harvesting power supply. While the charging voltage across the storing capacitor at a charging time of 90 min is 3.26 V (point *D*) from 0 V (as shown in Fig. 15), the electrical energy from the storing capacitor can be discharged into the wireless sensor node by using the instantaneous discharging circuit. The voltage across the wireless sensor node at the starting discharging time is 3.2 V (point *A*). During the operating time (620 ms) of the wireless sensor node, the voltage across the storing capacitor decreases to 3.22 V (point *E*). During the data transmission, the voltage across the wireless sensor node decreases to 3.1 V (point *C*). From Fig. 12, although the long charging time of 90 min is spent to charge the storing capacitor from 0 to 3.26 V in the incipient stage, it takes a shorter charging time of 4 min to charge the storing capacitor from 3.22 to 3.26 V in the next time duration.

The discharging energy of the instantaneous discharging circuit provided by the storing capacitor at one discharging period is

$$\begin{aligned} E &= \frac{\Delta(U^2)C}{2} = \frac{[(3.26V)^2 - (3.22V)^2] \times 0.47\mathrm{F}}{2} \\ &= 60.91\,\mathrm{mJ}. \end{aligned} \tag{22}$$

From (21) and (22), the instantaneous provided energy of the instantaneous discharging circuit is larger than the necessary minimum energy of the wireless sensor node in a working cycle ($E > W$). In the receiving time of 620 ms, the voltage across the storing capacitor decreases from 3.26 to 3.23 V. The calculated discharging power of the receiving state is 73.8 mW (>20 mW). In the transmitting time of 5 ms, the voltage across the storing capacitor decreases from 3.23 to 3.22 V. The calculated discharging power of the transmitting state is 3 W (>110 mW). The energy from the instantaneous discharging circuit can drive the operation of the wireless sensor node.

The electric-field energy harvesting with the upconversion oscillation circuit can drive the wireless sensor node with a peak output power of 110 mW at a zero-data-loss communication distance of 90 m.

Because the communication distance of the wireless sensor node with energy harvesting supply is short, a repeater should be placed at ground to send the receiving measured data to a specified server. According to general height of 10 kV power line and the communication distance of zero data loss, the distance between the repeater and the wireless sensor node must be less than 90 m.

V. Conclusion

In this paper, a noncontacting cylindrical harvester is designed for wireless-monitoring device, and a management circuit with upconversion oscillation technology is proposed to increase the energy harvesting efficiency. Power-frequency voltage signal across the harvester is transformed into the higher frequency signal with two oscillation frequencies in the switch-on/off time by using the upconversion circuit. We theoretically analyze the performance of the harvester and the upconversion method, and the experimental results present the similar trend of the theoretical results. In experiment, the maximum power and the maximum efficiency of the upconversion electric-field energy harvesting are 663 μW and 90.5%, respectively. Compared with traditional circuits for electric-field energy harvesting, the upconversion oscillation circuit with a small-size transformer can accumulate electric-field energy from a harvester more efficiently. In experiment, while the charging voltage across the storing capacitor at a charging time of 90 min is 3.26 V, the wireless sensor node can be driven with an output power of 110 mW at a communication distance of 90 m. This new principle of electric-field energy harvesting can meet the power supply requirement of the wireless sensor node. The extent of the power-line phase-to-ground rms voltage (u_o) for the management circuit is $1 - 30$ kV. When $u_o < 1$ kV, the control circuit with the power consumption of 6 μW is hardly driven by the harvester with the output power ($<$7 μW). When $u_o > 30$ kV, the switch is broken down and the upconversion oscillation circuit cannot work. The high-efficiency electric-field energy harvesting with the upconversion oscillation technology can be achieved at the lower power-line voltage ($u_o < 1$ kV) by using the lower power-consumption control integrated circuit. If the communication module with other communication protocol such as GSM or GPRS is used, a stronger electric-field source for energy harvesting is required. Furthermore, the capacitance of the storing capacitor $(C_{\rm st})$ in the management circuit must be larger to supply more energy for the communication module and to make the frequency of sending data higher. It can be used for batteryless wireless sensor networks to monitor some parameters such as temperature, icing of a high-voltage power line, and other potential applications for the smart grid.

Acknowledgment

The paper has been submitted solely to this journal and is not published, in press, or submitted elsewhere.

References

[1] B. T. Kuhn and R. S. Balog, "Design considerations for long-term remote photovoltaic-based power supply," in *Proc. IEEE Appl. Power Electron. Conf.*, Feb. 24–28, 2008, pp. 154–159.

[2] V. Raghunathan, A. Kansal, J. Hsu, J. Friedman, and M. Srivastava, "Design considerations for solar energy harvesting wireless embedded system," in *Proc. 4th Int. Symp. Inf. Process. Sens. Netw.*, Apr. 15, 2005, pp. 457–462.

[3] R. N. Torah, M. J. Tudor, K. Patel, I. N. Garcia, and S. P. Beeby, "Autonomous low power microsystem powered by vibration energy harvesting," in *Proc. IEEE Sens. Conf.*, Oct. 28–31, 2007, pp. 264–267.

[4] P. D. Mitcheson, T. C. Green, E. M. Yeatman, and A. S. Holmes, "Architectures for vibration-driven micropower generator," *J. Microelectromech. Syst.*, vol. 13, pp. 429–440, Jun. 2004.

[5] S. Meninger, J. O. Mur-Miranda, R. Amirtharajah, A. P. Chandrakasan, and J. H. Lang, "Vibration-to-electric energy conversion," *IEEE Trans. Very Large Scale Integr. (VLSI) Syst.*, vol. 9, no. 1, pp. 64–76, Feb. 2001.

[6] T.-K. Chung, D.-G. Lee, M. Ujihara, and G. P. Carman, "Design, simulation, and fabrication of a novel vibration-based magnetic energy harvesting device," in *Proc. Int. Solid-State Sens., Actuators Microsyst. Conf.*, Jun. 10–14, 2007, pp. 867–870.

[7] M. A. Weimer, T. S. Paing, and R. A. Zane, "Remote area wind energy harvesting for low-power autonomous sensors," in *Proc. IEEE Power Electron. Spec. Conf.*, Jun. 18–22, 2006, pp. 1–5.

[8] Y. K. Tan and S. K. Panda, "A novel piezoelectric based wind energy harvester for low-power autonomous wind speed sensor," in *Proc. 33rd Annu. Conf. IEEE Ind. Electron. Soc.*, Nov. 5–8, 2007, pp. 2175–2180.

[9] C. Park and P. H. Chou, "AmbiMax: Autonomous energy harvesting platform for multi-supply wireless sensor nodes," in *Proc. IEEE Commun. Soc. Conf. Sens. Ad Hoc Commun. Netw.*, Sep. 28, 2006, vol. 1, pp. 168–177.

[10] R. Myers, M. Vickers, H. Kim, and S. Priya, "Small scale windmill," *Appl. Phys. Lett.*, vol. 90, pp. 054106–1–054106-3, Jan. 2007.

[11] T. S. Paing and R. A. Zane, "Resistor emulation approach to low-power energy harvesting," in *Proc. IEEE Power Electron. Spec. Conf.*, Jun. 18–22, 2006, pp. 1–7.

[12] T. Le, K. Mayaram, and T. Fiez, "Efficient far-field radio frequency energy harvesting for passively powered sensor networks," *IEEE J. Solid-State Circuits*, vol. 43, no. 5, pp. 1287–1302, May 2008.

[13] D. Lin, W. Caisheng, L. Xianzhi, Y. Lijun, M. Yan, and S. Caixin, "A novel power supply of online monitoring system for power transmission lines," *IEEE Trans. Ind. Electron.*, vol. 57, no. 8, pp. 2889–2895, Aug. 2010.

[14] Z. Y. Wu, Y. M. Wen, and P. Li, "A power supply of self-powered online monitoring system for power cords," *IEEE Trans. Energy Convers.*, vol. 28, no. 4, pp. 921–928, Dec. 2013.

[15] H. Zangl, T. Bretterklieber, and G. Brasseur, "A feasibility study on autonomous online condition monitoring of high-voltage overhead power line," *IEEE Trans. Instrum. Meas.*, vol. 58, no. 5, pp. 1789–1796, May 2009.

[16] X. Zhao, T. Keutel, M. Baldauf, and O. Kanoun, "Energy harvesting for a wireless-monitoring system of overhead high-voltage power lines," *IET Gener. Transm. Distrib.*, vol. 7, no. 2, pp. 101–107, Feb. 2013.

[17] P. Li, Y. M. Wen, C. B. Jia, and X. S. Li, "A magnetoelectronic composite energy harvester and power management circuit," *IEEE Trans. Ind. Electron.*, vol. 58, no. 7, pp. 2944–2951, Jul. 2011.

[18] P. Li, Y. M. Wen, P. G. Liu, X. S. Li, and C. B. Jia, "A magnetoelectronic energy harvester and management circuit for wireless sensor network," *Sens. Actuators A, Phys.*, vol. 157, no. 1, pp. 100–106, Jan. 2010.

[19] P. Li, Y. M. Wen, W. J. Yin, and H. Z. Wu, "An upconversion management circuit for low-frequency vibrating energy harvesting," *IEEE Trans. Ind. Electron.*, vol. 61, no. 7, pp. 3349–3358, Jul. 2014.

[20] G. K. Ottman, H. F. Hofmann, A. C. Bhatt, and G. A. Lesieutre, "Adaptive piezoelectric energy harvesting circuit for wireless remote power supply," *IEEE Trans. Power Electron.*, vol. 17, no. 5, pp. 669–676, Sep. 2002.

Authors, photographs, and biographies not available at the time of publication.